Journal of Pharmaceutical Sciences 113 (2024) 2394–2404

Contents lists available at ScienceDirect

Journal of Pharmaceutical Sciences

journal homepage: www.jpharmsci.org

Pharmaceutics, Drug Delivery and Pharmaceutical Technology

Comparison of Protein-like Model Particles Fabricated by Micro 3D Printing to Established Standard Particles

Ilias Amara[a,b,c,1], Oliver Germershaus[b,*], Christopher Lentes[a,*], Steffen Sass[d], Stephany Mamdjo Youmto[d], Jan Olaf Stracke[e], Mirjam Clemens-Hemmelmann[a], Anacelia Assfalg[e,2]

[a] *Pharmaceutical Development & Supplies, Pharmaceutical Technical Development Biologics Europe, F. Hoffmann-La Roche, Grenzacherstrasse 124, 4070 Basel, Switzerland*
[b] *Institute of Pharma Technology, School of Life Sciences, University of Applied Sciences Northwestern Switzerland, Hofackerstrasse 30, 4132 Muttenz, Switzerland*
[c] *Department of Pharmaceutical Sciences, University of Basel, Klingelbergstrasse 50, CH-4059 Basel, Switzerland*
[d] *Pharma Technical Development, Roche Diagnostics GmbH, Nonnenwald 2, 82377 Penzberg, Germany*
[e] *Analytical Development and Quality Control, Pharmaceutical Technical Development Biologics Europe, F. Hoffmann-La Roche, Grenzacherstrasse 124, 4070 Basel, Switzerland*

ARTICLE INFO

Article history:
Received 16 December 2023
Revised 9 April 2024
Accepted 9 April 2024
Available online 12 April 2024

Keywords:
Protein particle
Biopharmaceutical formulations
Subvisible particles
Visible particles

ABSTRACT

Innovative analytical instruments and development of new methods has provided a better understanding of protein particle formation in biopharmaceuticals but have also challenged the ability to obtain reproducible and reliable measurements. The need for protein-like particle standards mimicking the irregular shape, translucent nature and near-to-neutral buoyancy of protein particles remained one of the hot topics in the field of particle detection and characterization in biopharmaceutical formulations. An innovative protein-like particle model has been developed using two photo polymerization (2PP) printing allowing to fabricate irregularly shaped particles with similar properties as protein particles at precise size of 50 μm and 150 μm, representative of subvisible particles and visible particles, respectively.

A study was conducted to compare the morphological, physical, and optical properties of artificially generated protein particles, polystyrene spheres, ETFE, and SU-8 particle standards, along with newly developed protein-like model particles manufactured using 2PP printing.

Our results suggest that 2PP printing can be used to produce protein-like particle standards that might facilitate harmonization and standardization of subvisible and visible protein particle characterization across laboratories and organizations.

Introduction

Regulatory authorities and pharmacopeias demand data regarding the presence of particles in parenteral formulations, along with evidence of measures taken to limit, control, and identify them. This is essential due to their potential impact on patient safety, drug product efficacy, and stability.[1]

While injectable drug products often contain particles of varying sizes, they are typically categorized as either visible or sub-visible. Visible particles are those that can be detected by the unaided human eye without additional magnification.[2] Studies have shown that under optimal conditions, trained inspectors using pharmacopeial inspection methods can reliably detect particles with 70% efficiency when they reach sizes of 150 μm.[2] However, it's important to note that this threshold of 150 μm represents ideal conditions, and that any deviations in the matrix solution, container, or particle property may result in a shift in the visible detection threshold beyond this value.[3] Furthermore, particles differ with regards to their chemical composition and can be categorized as inherent, intrinsic or extrinsic according to their origin.[4]

All drug products for parenteral administration must be "essentially free" or "practically free" of visible particles and must comply

* Corresponding authors.
E-mail addresses: oliver.germershaus@fhnw.ch (O. Germershaus), christopher.lentes@roche.com (C. Lentes).
[1] Current affiliation: Device and Packaging Development, Pharmaceutical Technical Development Biologics Europe, F. Hoffmann-La Roche, Grenzacherstrasse 124, 4070 Basel, Switzerland.
[2] Current affiliation: Roche Pharma Research and Early Development, pRED Informatics, Roche Innovation Center Basel, F. Hoffmann−La Roche Ltd., Basel, Switzerland.

https://doi.org/10.1016/j.xphs.2024.04.011

with limit tests for subvisible particle count.[5] The tests and requirements pertaining subvisible particles are harmonized across major pharmacopoeias, stating that these particles should be controlled within the size range ≥ 10 μm and ≥ 25 μm using light obscuration (LO) or membrane microscopy (USP <787> and <788>, EP 2.9.19, and JP 6.07). Polystyrene (PS) spheres of well-defined size and concentration are required for calibration of these methods.[6] The same applies to the system suitability tests, where PS spheres are used to validate the correct functioning of the instruments/methods prior to use.

Flow imaging microscopy (FIM) is often used as an orthogonal method for counting and sizing of visible and subvisible particles. FIM provides micrographs of all particles detected, allowing identification and/or classification of particles, supporting root cause analysis. Another advantage of FIM is its application over a wide range of sizes, from approximately 2 μm up to several hundred micrometers, by choosing the instrument configuration such as flow cell depth and objective magnification. Calibration and evaluation of these instruments is mainly performed using PS spheres. These particles are perfectly spherical and are characterized by high optical contrast, due to the high refractive index difference between PS and aqueous solutions. These characteristics render PS spheres easily detectable by analytical instruments and allow simple and unequivocal size determination. Protein particles pose a distinct challenge for instruments due to their irregular shape and transparent nature. This is primarily attributed to the inherently low refractive index difference between protein particles and the surrounding aqueous protein formulation.[7]

Several studies have demonstrated that calibrating analytical instruments with particles having a lower optical contrast as compared to the matrix fluid increases their sensitivity. This enhancement leads to more precise sizing and counting capabilities.[8] In addition, the difference in sensitivity between LO and FIM has been studied several times showing substantially higher detectability of protein particles with FIM.[9,10]

Ripple et al. reported that FIM instruments from different manufacturers as well as different instrument configurations result in statistically significant differences with regards to particle counts.[11] The use of a suitable reference material may reduce variability in protein particle counting between FIM instruments without affecting sizing accuracy of polystyrene spheres.[12] Calibration of analytical instruments to achieve the same sensitivity is crucial to improve repeatability of particle sizing and counting, especially for orthogonal methods like FIM.

Concerning visible particles, comprehensive inspection programs are implemented to control and monitor their presence ensuring that each batch is “essentially free” or “practically free” of visible particles or “without visible particles, unless otherwise justified” as described in USP <1>, <790> and EP 2.9.20. Visual inspection is used to identify the presence or absence of visible particles in final drug products and can be performed in a manual, semi-automatic or fully automated way. The use of training kits composed of particles of different types and sizes typically found in products is necessary for the training of human inspectors as well as for the evaluation of the performance and qualification of inspection machines.[2] These training kits are mainly composed of intrinsic and extrinsic particles. Companies may in addition produce or collect representative samples with typical protein particles to better train human inspectors. These in-house protein particle training kits are convenient but their composition is difficult to standardize with regards to absolute protein particle concentration and size distribution and their stability over time remains problematic.[13,14] Proper training of human inspectors not only leads to improved detection but also accurate recognition of these protein particles, enabling optimal quality control.[15] Sample sets composed of containers having different protein-like particle concentrations have also been used to semi-quantitatively assess the amount of protein particles in a closed container.[14,16]

With regards to both subvisible and visible particle characterization in biopharmaceutical products, the need for particle standards with physical and optical properties similar to protein particles is very high.[17] The scientific community has been working on development of such particles for over 10 years. The National Institute of Standards and Technology (NIST) has developed an abrasion process for ethylene tetrafluoroethylene (ETFE) tubes to create polydisperse particles with optical contrast and morphology similar to protein particles.[18] Furthermore, a photolithography-based process using SU-8 photosensitive polymer has been established for the fabrication of monodisperse visible particle with irregular shape.[19] However, ETFE particles are characterized by fast sedimentation and their size distribution is difficult to control, while SU-8 particles have received mixed ratings as visible protein particle standard due to their high reflectivity and sharp edges.[13]

Herein, a new method for the preparation of protein-like particles is explored. The use of micro 3D printing by two photon polymerization (2PP) enables the fabrication of microstructures with resolution in the range of 200 nanometers.[20] Micro 3D printing allows production of a defined number of particles with precise size and shape, while offering complete flexibility on their morphology by definition of the 3D structure to be printed. The physical, optical and mechanical attributes of the produced particles are controlled by the choice of photoresins and 3D models employed. Moreover, the flexibility offered by micro 3D printing could allow the fabrication of a protein-like particle set covering the variability of protein particles found in typical protein formulations.

A comparative study including polystyrene spheres, protein-like standard particles developed by NIST (ETFE and SU-8) as well as four configurations (two 3D models and two photoresins) of protein-like model particle fabricated with micro 3D printing has been conducted to evaluate the suitability of the different particle types as protein-like model particles. Morphology, optical properties and image similarity of the different particle standards and protein-like model particles, in the subvisible and visible range, were compared with a protein particle data set reflecting its variability. A method to adjust the optical contrast of protein-like model particles is presented to further improve their similarity to protein particles.

Materials and Methods

Particles

Polystyrene Spheres

Duke Standards™ 4000 Series uniform polymer microsphere size standards of 50 μm (mean diameter - NIST traceable: 50.2 μm ± 1.0 μm) and 160 μm (mean diameter - NIST traceable: 160 μm ± 3.0 μm) were purchased from Thermo Fisher Scientific (Waltham, MA, USA).

NIST Standard Particles

Suspensions of ethylene tetrafluoroethylene (ETFE) particles for size distribution and morphology (NIST Reference Material 8634) were purchased from NIST (Gaithersburg, MD, USA) and stored at 2-8°C. The reference value for the aspect ratio has a mean value of 0.568 ± 0.069 and a standard deviation of 0.143 ± 0.017.[18]

Suspensions of 250 μm length SU-8 particles were provided by NIST (Gaithersburg, MD, USA) and stored at 2-8°C. The aspect ratio of these SU-8 particle standards is 0.6.[19]

Preparation of Micro 3D Printed Protein-Like Model Particles

Two 3D models of protein-like particles, each with a distinct morphology and aspect ratio, were designed using computer-aided design (CAD) software, using actual protein particles found in a drug product as the template. The first model, designated as model A,

represents an elongated structure with non-constant low thickness. The second model, designated as model B, represents a compact, more globular structure. The length of the protein-like model particles (PLMP), defined as the maximum distance between two points belonging to the 3D model, was set at 50 μm for the subvisible range and 150 μm for the visible range.

Fabrication of protein-like model particles (PLMP) was performed by dip-in laser lithography using a two-photon polymerization (2PP) printer Photonic Professional GT (Nanoscribe, Karlsruhe, Germany). The microscope objective Plan-Neofluar 25x/0.8 Imm Corr DIC (Carl Zeiss, Oberkochen, Germany) was used to focus the laser. Particles were printed on a 25 $\times$ 25 mm ^{2} indium tin oxide (ITO) coated glass substrate with a thickness of 700 μm.

Two proprietary photoresins (Nanoscribe, Karlsruhe, Germany) having different refractive indexes and densities were used to print PLMPs: IP-S (RI = 1.51; ρ= 1.11 g/mL) and IP-PDMS (RI = 1.45; ρ = 1.05 g/mL). For each model, the fabrication parameters were optimized to reduce the printing time while maintaining good resolution.

Protein Particles from Biopharmaceutical Formulations

Representative protein particles were generated using two monoclonal antibodies: mAb 1 (F. Hoffmann-La Roche Ltd, Basel, Switzerland), at 50 mg/mL formulated in 20 mM Histidine/Histidine-HCl, 240 mM Sucrose, 0.05% Poloxamer 188 at pH 6, and mAb 2 (F. Hoffmann-La Roche Ltd, Basel, Switzerland), at 5 mg/mL formulated in 20 mM Histidine/Histidine-HCL, 240 mM Sucrose, 10 mM Methionin, 0,05% Polysorbate 20 at pH 5.5.

A dataset comprising four hundred images and properties of protein particles was gathered through flow imaging microscopy. These particles originated from mAb formulations subjected to various stress conditions (freeze/thaw, 5°C, 25°C, inverted vials) and assessed at different time points (3, 6, 12, 24, 36 months) during stability studies. This dataset captures the wide variety of typical protein particles found in biopharmaceutical formulations.

Based on the size of PLMP, collected data were separated into two size classes representing subvisible particles (33.5 μm $\leq$ X $\leq$ 66.5 μm) and visible particles (100 μm $\leq$ X $\leq$ 200 μm). These size ranges correspond to the size of the PLMP $\pm$ 30%.

Preparation of Particle Suspensions

Protein Matrix

Formulation of mAb 1 (composition described in section 2.1.4) was filtered using membrane filters with a pore size of 0.22 μm (Millex-GV Syringe Filter Unit. Merck Millipore, Cork, Ireland) to obtain a protein solution free of subvisible or visible particles. This matrix fluid is representative of a typical protein formulation in terms of optical and physical properties and is referred hereafter as protein matrix. Its refractive index was measured to be 1.355 and density 1.047 g/cm^3 at 20°C.

Matrix Fluids for Variation of Refractive Index

Solutions of various refractive indexes (RI = 1.39, 1.42, 1.45, 1.48 and 1.51) were prepared by dilution of 2-pyridinemethanol at various concentration (2-PM, 98%, Sigma Aldrich Chemie GmbH, Steinheim, Germany) in ultrapure water (MilliQ, Millipore, Molsheim, France), containing 0.05% Poloxamer 188.

Particle Suspensions

To prevent contamination and changes in the refractive index of the solution, 6 mL glass vials were cleaned with ultrapure water and blow-dried with filtered air. Next, 2 milliliters of either the protein formulation or the 2-PM solutions were manually filled into the vials using a 5-mL syringe (5mL Luer-Lok Syringe, BD, Laagstraat, Belgium) with a 0.22-μm polyvinylidene difluoride (PVDF) Millex GV membrane filter (Merck Millipore, Cork, Ireland) connected to it. Particle standards were transferred into the containers using a pipette for PS spheres, ETFE, and SU-8 particles, and a metallic needle for PLMPs. Twenty to thirty of each type of standard particles were introduced in individual containers.

Refractometry

The refractive indices of the matrix fluids were measured at 20°C and at λ = 589 nm using a digital refractometer (DR6300-T, A. Krüss Optronic GmbH, Hamburg, Germany).

The instrument's performance was evaluated with ultrapure water, confirming a refractive index of 1.33 at a temperature of 20°C and a wavelength of 589 nanometers.

Flow Imaging Microscopy

Images of suspended particles were acquired using FlowCam 8100 (Yokogawa Fluid Imaging Technologies, USA) equipped with a 300 μm flow cell and using a 4x magnification objective resulting in a resolution of 1.875 μm/pixel. The flowrate was set at 1.0 mL/min and the auto image rate at 320 frames per second enabling an efficiency at 132.1 %. The efficiency was set exceptionally high in order to maximize data collection, enabling the capture of multiple images of the same particle with varying orientations within the flow cell. Duplicate images of the same particle with identical orientations were subsequently removed. The detection threshold for dark pixels was set at 18 and at 15 for white pixels. Prior to sample analysis, the system underwent thorough cleaning with multiple cycles involving a detergent followed by rinsing with ultrapure water. For every measurement conducted with a specific refractive index matrix, the flow cell was rinsed with a particle-free solution matching the refractive index. This was done to prevent any variations in refractive index of the sample during the measurement. Blank assessment was performed regularly to maintain cleanliness of the flow cell. Homogenization of the particle suspensions with gentle inversion was done prior to the measurement. The contents of each vial was carefully withdrawn using a volumetric pipette and directly transfered into FlowCam.

Visual Spreadsheet software (Yokogawa Fluid Imaging Technologies, USA) was used to capture particle images and obtain morphological descriptors of each particle. The particle images were sorted based on their length parameters. This was done to facilitate the detection of the standard particle images, as their sizes were known.

Aspect ratio was determined by division of the width of a particle by its length. Length and width were determined as maximum and minimum value of measurement of Ferets diameter at 36 angles, respectively.

Analysing the particle intensity value provides insight into the translucency of the particles. The intensity value of particle images obtained with FlowCam directly correlates with particle transparency. The intensity value determined in flow imaging microscopy represents the average grayscale value of all pixels making up the detected particle boundaries. The average background intensity was set at 170 gray levels, in accordance with the supplier's recommendations for the analysis of translucent protein-like particles in flow cell images. The intensity value ranges from 0 (being black) to 255 (being white), meaning that a higher intensity indicates greater transparency of the particle.

Statistical Analysis

Data sets were tested for normality using D'Agostino and Pearson normality test using a p value $\geq$ 0.05. Data sets were statistically analyzed using one-way ANOVA using Kruskal-Wallis test and Dunn's

post test performed for multiple comparisons with protein particles defined as the reference. Statistical analysis was performed using Prism (GraphPad Software, San Diego, CA, USA).

Siamese Neural Network

A Siamese Neural Network (SNN) was implemented to compare the similarity of particle standard images with protein particle images in an unbiased manner. The network architecture, developed using Python with Keras and TensorFlow libraries, involves two identical Convolutional Neural Network (CNN) subnetworks for processing each input image. Each subnetwork concludes with a fully connected layer, enabling the computation of Euclidean distance between the outputs of these layers. The resulting distance is then transformed using a sigmoid activation function to determine similarity, scaling the similarity scoring between 0 and 1.

Particle images from the raw FlowCam data were cropped to obtain individual particle images. A dataset of four hundred protein particles images, described in section 2.1.4, was collected as input images. These images were categorized into two distinct groups based on the particle size range: subvisible and visible. Additionally, five images of subvisible and visible particles from each standard particle (PS spheres, ETFE, SU-8, and PLMPs), both in the protein matrix and in matrix fluids with different refractive indices, were also selected as input images.

Positive pairs, containing two images of the same particle type, and negative pairs, containing two images of different particle types, were generated and manually labelled. These pairs constitute the training data, enabling the Siamese neural network to learn similarity by presenting pairs of images to individual subnetworks.

Approximately three thousand image pairs were used as inputs data, 70% for training, 15% for validation, and 15% for testing. The trained model achieved an accuracy of 90% on the validation dataset. The model was then deployed to assess similarity between untested image of particle standards and images of protein particles.

For further details on the Siamese neural network, please refer to supplementary information and Fig. S1.

Results

Visual Assessment

Commercially available particle standards and PLMPs fabricated with two different photoresins (Fig. 1) were suspended in protein matrix formulation and analyzed by FIM. Representative flow imaging micrographs are shown in Fig. 2, categorized as subvisible particles ($\leq$ 100 μm for particle standard and specific range for protein particle, see section 2.1.4) and visible particles ($>$ 100 μm for particle standard and specific range for protein particle, see section 2.1.4).

Protein particles, both in the subvisible and visible range, are typically described as having an irregular shape and being partially translucent.[21] In addition, protein particles exhibit a range of morphological and optical variations.[8] The representative mAb protein particles shown in Fig. 2 align with this overall description, displaying characteristics such as irregular shape, partial translucency, and variability.

PS spheres are designed to have very regular spherical shape and appear very dark due to their high refractive index of RI = 1.58.[22] The standards developed by NIST consist of two types: ETFE for the subvisible size range (although it is possible to find some particles with larger sizes) and SU-8 for the visible size range. Despite the fact that some ETFE particles created by abrasion have sharp edges, the vast majority of particles show an irregular shape, similar to protein particles.[18] In addition, their low refractive index (RI = 1.41) results in highly transparent particles, which may appear even more transparent than protein particles. Regarding SU-8 particles, masks used for manufacturing result in an irregular shape, but particles have sharp contours, unlike protein particles.[19] Despite the high refractive index of SU-8 material (RI= 1.6), the low thickness and porosity of the SU-8 particles result in an optical density and contrast similar to protein particles.

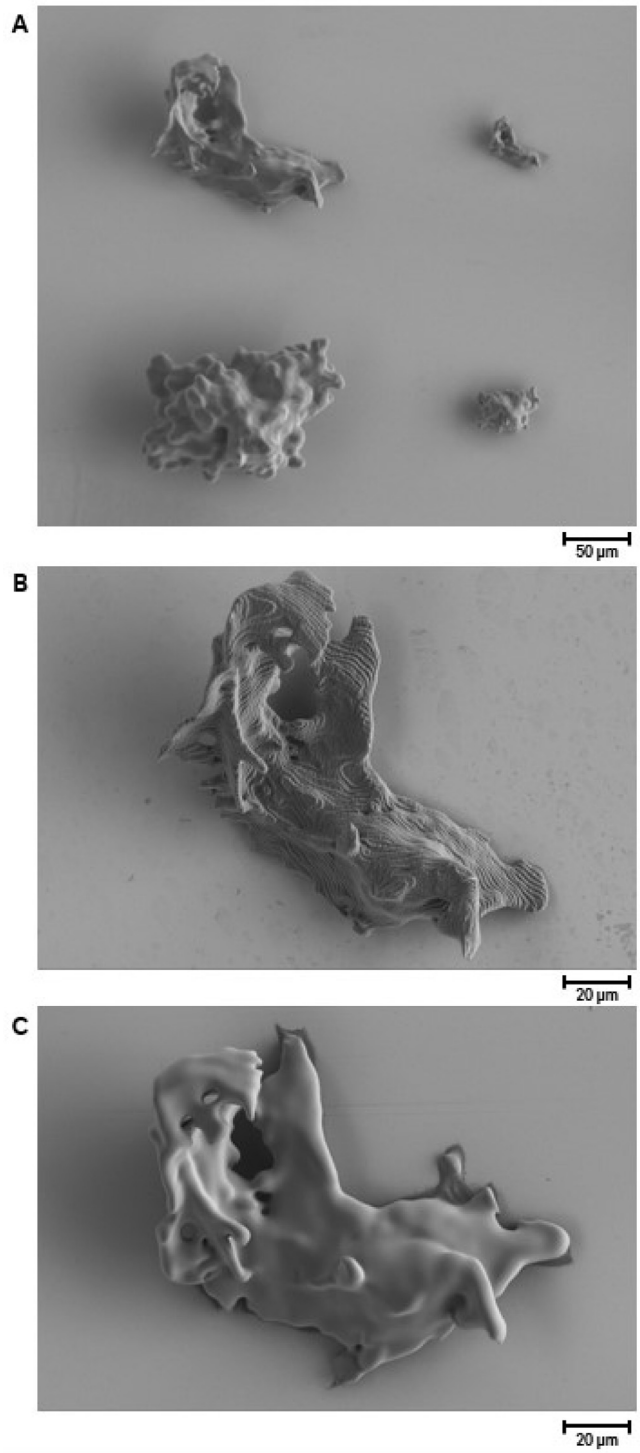

Figure 1. A) Scanning electron micrograph of the four PLMP configurations (top left: Model A, 150 μm length; top right: Model A, 50 μm length; bottom left: Model B, 150 μm length; bottom right: Model B, 50 μm length) fabricated using IP-S by 2PP printing. B) Scanning electron micrograph of PLMP (Model A, 150 μm length) made of IP-S. C) Scanning electron micrograph of PLMP (Model A, 150 μm length) made of IP-PDMS.

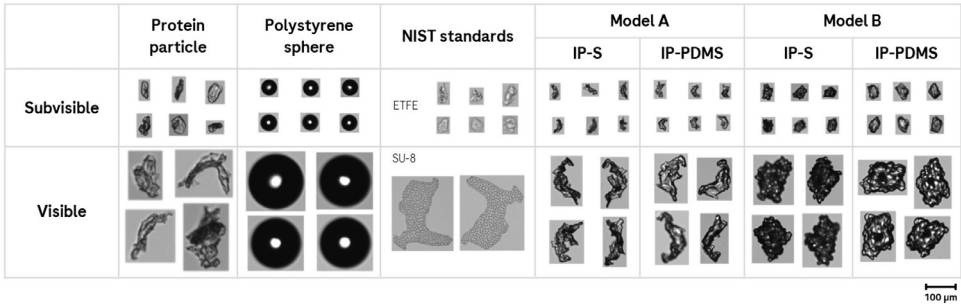

Figure 2. Representative images obtained by flow imaging microscopy of protein particles, PS spheres, NIST standard particles and PLMP. All particles were measured using the same flow imaging microscopy settings and suspended in protein matrix formulation.

The flexibility offered by 2PP printing with regards to design of the models to be printed allows to produce particles with morphologies similar to protein particles. The two models used in this study are characterized by their irregular shapes, with Model A corresponding to elongated protein particles with lower thicknesses and Model B representing compact and more spherical particles. A difference in transparency can be observed between the four PLMP configurations which is related to the thickness of the structures as well as the refractive index of the photoresins used. The variation of the optical contrast will be described in more detail in the following sections. The SEM images presented in Fig. 1B and 1C show a difference in surface quality between the two types of photoresins used. The IP-S photoresin allows printing with high detail resolution while the IP-PDMS results in slightly lower resolution and a smoother surface.

Aspect Ratio

Aspect ratios given in Fig. 3 show that both, subvisible and visible protein particles show a high variability in shape ranging from near spherical (maximum aspect ratio 0.97) to elongated shape (minimum aspect ratio 0.08). The median value of aspect ratios is 0.54 for subvisible protein particles and 0.46 for visible protein particles, which corresponds to the range typically observed for protein particles.[23]

The aspect ratios of PS spheres correspond to almost perfect spheres (median aspect ratio of 0.98 and 0.99 for subvisible and visible particles, respectively) with standard deviation < 0.02. Statistical analysis reveals highly significant differences (adjusted P value < 0.0001) between the aspect ratios of protein particles vs. PS spheres for both subvisible and visible size range.

The manufacturing process of ETFE particles allows to generate particles with an aspect ratio having a range and variability similar to that of protein particles. The aspect ratio values shown in Fig. 3A match the certification of this reference material by NIST, indicating agreement between our measured results and NIST's reference values.[18] For SU-8 particles, it is possible to have control over the 2D morphology of these particles by designing the shape of the masks used during fabrication. Their flat shape results in a preferred orientation in the flow cell, such that the particle's smallest surface area is oriented towards the direction of fluid flow. This is evident in Fig. 3B where the value of the aspect ratio corresponds to that of the mask used with very small variation.[13]

The median aspect ratios for Model A, which represents an elongated particle, ranged from 0.48 (IP-S) to 0.59 (IP-PDMS). For Model B, representing a more spherical particle, the median aspect ratios varied between 0.68 (IP-S) and 0.70 (IP-PDMS). Statistical analysis showed no significant differences between the aspect ratio of protein particles as compared to that of the 2PP printed particles.

It is important to note that the orientation of the non-spherical particles in the flow cell will influence the aspect ratio measured. Larger, non-spherical particles in the visible range assume a preferred orientation due to the flow of the solution inside the flow cell, resulting in lower standard deviation of measured aspect ratios (Fig. 3B, SU-8 and Model A particles). Particles in the subvisible range show a larger variation of measured aspect ratios since they are more subject to random orientation in the flow cell. Additionally, differences between particles of the same 3D shape but produced using different photoresins were observed, which might be due to different printing resolution or surface smoothness (Fig. 1B and 1C).

Optical Contrast

Protein particles are commonly defined by their semi-transparency and their refractive index, which closely matches that of protein formulations.[12] Biopharmaceutical formulations are aqueous

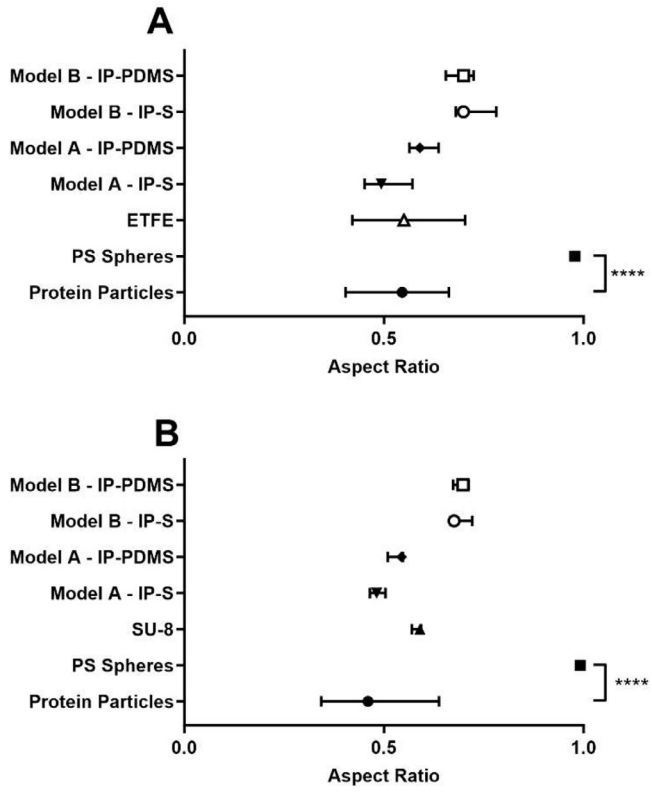

Figure 3. Median and interquartile range of aspect ratios determined by flow imaging microscopy of A) subvisible and B) visible particles suspended in protein matrix formulation. Asterisks indicate statistical significance (P value ≤0.0001: ****).

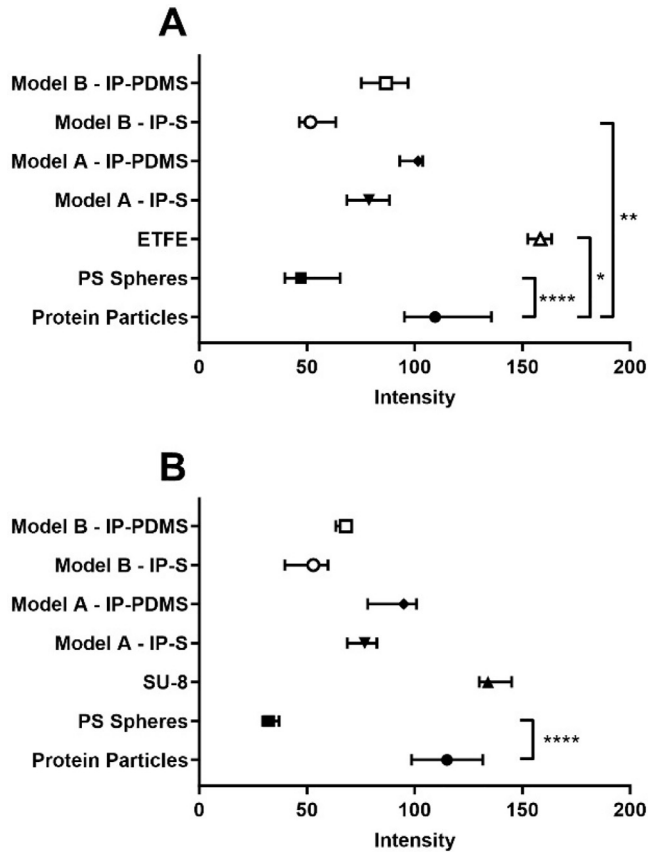

Figure 4. Median and interquartile range of particle intensities determined by flow imaging microscopy of A) subvisible and B) visible particles suspended in protein matrix formulation. Asterisks indicate statistical significance (P value ≤0.05: *; ≤0.01: **; ≤0.0001: ****).

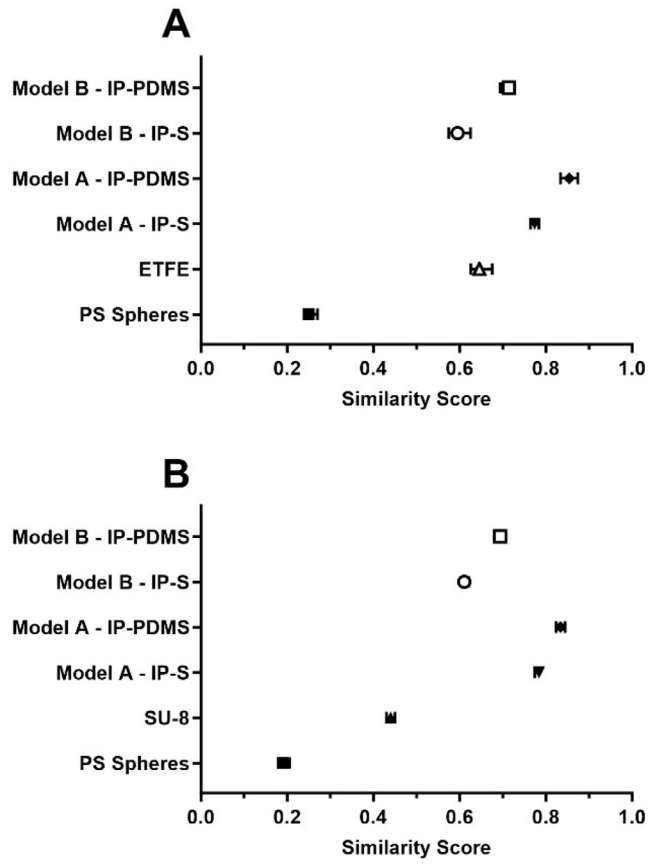

Figure 5. Median and interquartile range of particle image similarity score obtained with Siamese neural network of A) subvisible and B) visible particles suspended in Protein matrix formulation.

solutions with refractive indices ranging from 1.33 to 1.6, due to high protein concentration and/or presence of excipients such as sucrose at high concentration.[24] The refractive index of protein particles in monoclonal antibody formulations is reported to be RI = 1.41.[8,25]

The intensity values of particle standards were determined using flow imaging microscopy (Fig. 4) and were used to evaluate optical contrast of particles in biopharmaceutical formulations. The median intensity values for subvisible and visible protein particles were 109.5 and 115.1, respectively, confirming their high transparency.

The intensity values for PS spheres were the lowest among all particle types and showed a statistically significant difference from the intensity of protein particles, both for subvisible and visible particles (adjusted P value < 0.0001). The greater variability in intensity values for subvisible PS spheres could be attributed to the fact that some of the 50 μm diameter PS spheres were not in focus within the 300 μm depth flow cell.

The choice of using ETFE for particle standard fabrication by NIST was specifically based on its low refractive index (RI = 1.41), which is similar to the refractive index of protein particles. Nevertheless, ETFE particles were found to have significantly higher intensity values (median intensity of 158.4) than protein particles. On the other hand, refractive index of SU-8 (RI = 1.6) is higher than the refractive index of protein particles, but the low thickness and the porosity of SU-8 particles resulted in similar intensity values (median intensity of 134) as protein particles.

PLMPs displayed slightly lower intensity values compared to protein particles. This can be attributed to the higher refractive indexes of the photoresins used in 2PP printing as opposed to protein particles. Additionally, the thickness of the material affects the intensity and transparency of the particles. Model A, made of IP-PDMS, demonstrated the highest similarity to protein particles in terms of intensity values, with medians of 101.6 for subvisible and 95 for visible particles.

Image Similarity

The use of machine learning algorithms is becoming increasingly common to classify particle images acquired by flow imaging microscopy instruments.[23] The similarity between the images of protein particles and other particles was evaluated using a neural network-based algorithm (Fig. 5).

PS spheres obtained the lowest similarity score with a median value of 0.25 for subvisible and 0.19 for visible particles, confirming the lack of similarity to protein particles as observed with regards to visual assessment, aspect ratio and intensity. The particles developed by NIST resulted in a moderate median similarity scores of 0.64 for ETFE particles and 0.44 for SU-8 particles. The highest similarity score was obtained for PLMP Model A printed with IP-PDMS with a median value of 0.85 for the subvisible 0.83 for the visible particles. This result confirms the observations made in the previous sections where this PLMP configuration had mean intensity and mean aspect ratio values very similar to that of protein particles. Furthermore, the difference observed between particles prepared from IP-PDMS and IP-S were corroborated by similarity analysis, showing generally lower similarity for IP-S.

Effect of Variation of the Refractive Index of the Matrix Solution

Previous studies have shown that decreasing the absolute value of the refractive index difference (|ΔRI|) between particles and matrix

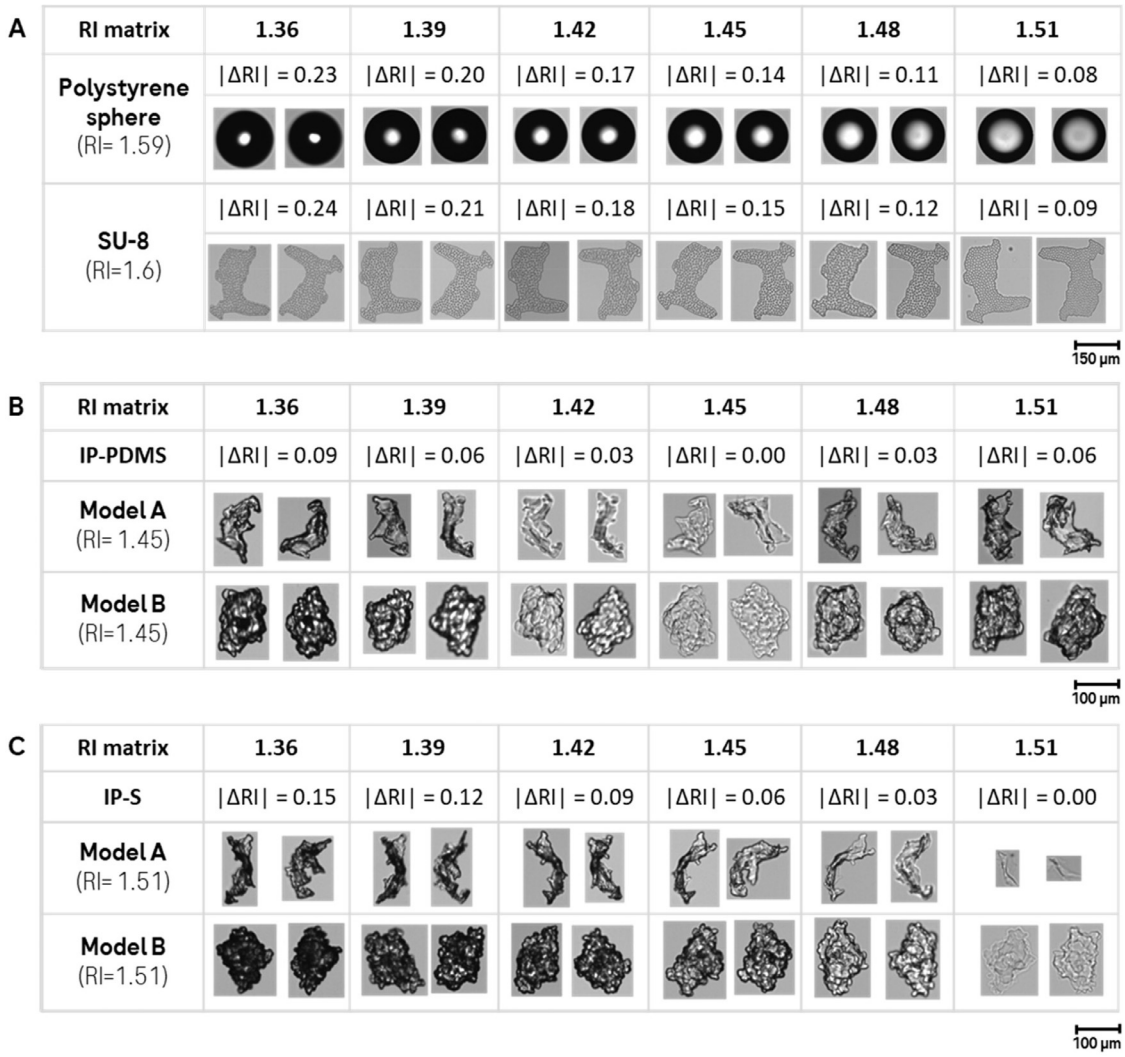

Figure 6. Representative flow imaging micrographs of A) PS sphere and SU-8 particles, B) PLMPs made of IP-PDMS, and C) PLMPs made of IP-S, introduced in matrix solution having different refractive indexes.

solution resulted in decreasing optical contrast between particles and surrounding medium, as well as a reduction in the particle diameters determined by FIM or LO.[26] Moreover, in protein formulations, the ΔRI for protein particles has been observed to be as low as 0.06.[8] Fig. 6 provides a visual representation of the effect of |ΔRI| variation on the appearance of various particles standards by adjusting the refractive index of the matrix solution.

Despite a minimum |ΔRI| of 0.08 for PS spheres and 0.09 for SU-8 particles at RI matrix of 1.51, no effect of ΔRI variation on the shape of the particles could be observed. Furthermore, there was no reduction in PS spheres diameter size, as shown in Fig. 7. However, it was noticed that with decreasing |ΔRI| the appearance of PS particles changed with a bright spot appearing in the centre of the particle image, whose diameter increased with decreasing |ΔRI|. This observation is supported by the mean intensity values of the PS spheres shown in Fig. 8A which increased from 33.2 to 61.4 with decreasing |ΔRI|. No substantial changes of appearance (Fig. 6), length (Fig. 7) or intensity value (Fig. 8A) were seen for SU-8 particles despite the variation of the refractive index.

The appearance of PLMPs of different shapes, produced by 2PP using two different polymers, changed substantially with variation of |ΔRI| (Fig. 6). For both polymers (IP-S and IP-PDMS), the highest particle transparency was observed when ΔRI = 0 (Fig. 8B and C) along with a significant reduction in particle length (expect for Model B IP-PDMS) (Fig. 7B and C).

Furthermore, the shape of the particles also influenced their appearance with variation of |ΔRI|. In general, Model A particles appeared more transparent, resulting even in only partial registration of particles in the case of IP-S Model A particles at ΔRI = 0 (Fig. 6). This observation is confirmed by the considerable drop in mean particle length to 59.2 μm. These findings were also supported by evaluation of particle intensity values (Fig. 8B and C). Similarly, for both polymers, the intensity values were lower for Model B compared to Model A. Therefore, by carefully designing particle geometry and strategically optimizing the refractive index of the matrix fluids, it becomes possible to generate standard particles that closely mimic the appearance of protein particles while accurately representing their natural variability.

The similarity scores of PS spheres, SU-8 particles and PLMPs, as shown in Fig. 9 corroborate the trends observed when analyzing particle intensities (Fig. 8). In general, we found that the similarity scores of PLMPs remained high with little variation across various ΔRI values, reaching maximum similarity at ΔRI = 0.

Median similarity scores for particles prepared from IP-PDMS or IP-S were comparable at equivalent |ΔRI| (Fig. 9D), indicating that the refractive index difference between the different polymers mainly

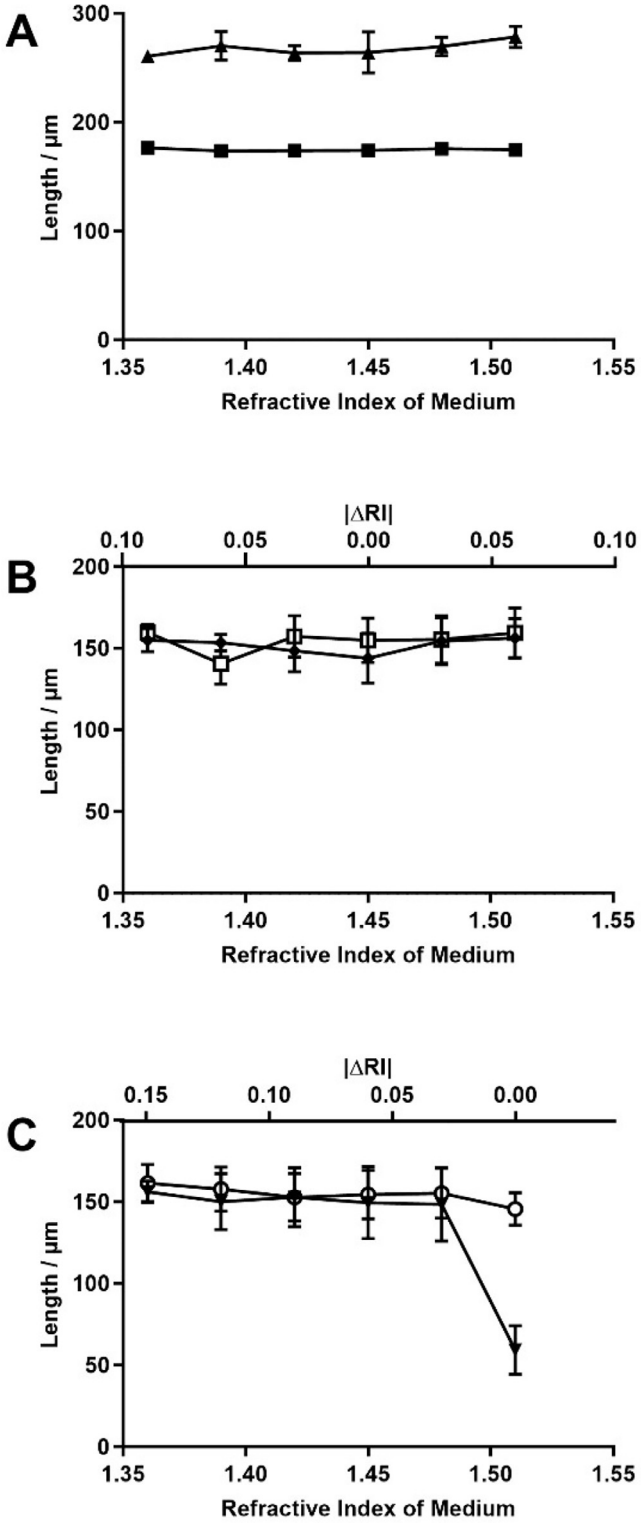

Figure 7. Effect of variation of the medium refractive index on particle length determined by flow imaging microscopy. A) PS spheres (filled squares, RI = 1.59), SU-8 (upward triangles, RI = 1.60). B) Particles produced by 2PP printing made of IP-PDMS (RI = 1.45, filled diamonds: Model A, open squares: Model B). C) Particles produced by 2PP printing made of IP-S (RI = 1.51, downward triangles: Model A, open circles: Model B).

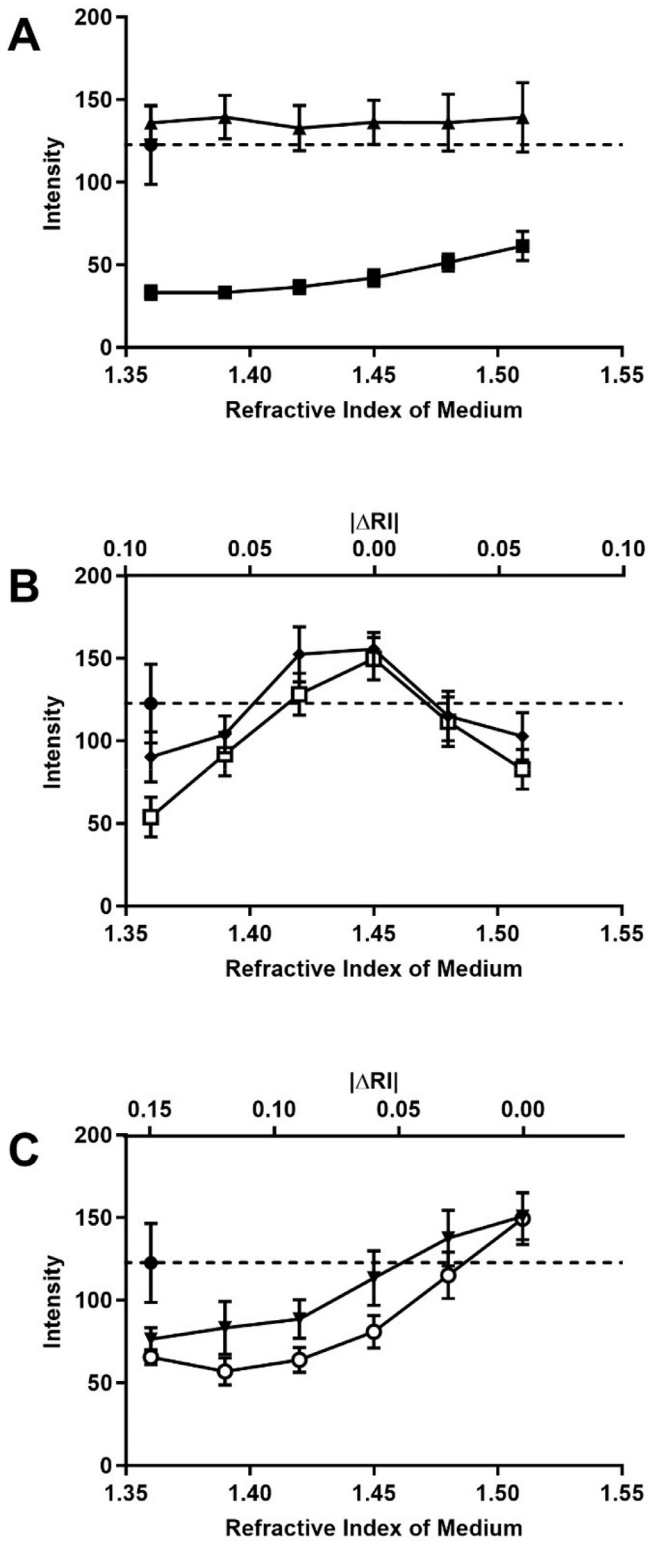

Figure 8. Effect of variation of the medium refractive index on particle intensity determined by flow imaging microscopy. A) PS spheres (filled squares, RI = 1.59), SU-8 (upward triangles, RI = 1.60) and protein particles (filled circle, intensity identified by dashed line in panel A - C). B) Particles produced by 2PP printing made of IP-PDMS (RI = 1.45, filled diamonds: Model A, open squares: Model B). C) Particles produced by 2PP printing made of IP-S (RI = 1.51, downward triangles: Model A, open circles: Model B).

affects particle appearance and similarity to proteinaceous particles. In addition, the particle design (model A or model B) affected similarity scores, with model A particles showing overall higher similarity than model B particles.

Interestingly, the image similarity score of SU-8 particles decreased despite the reduction of ΔRI. Detailed analysis of particle images (Fig. 6) shows that the negative impact on the similarity score

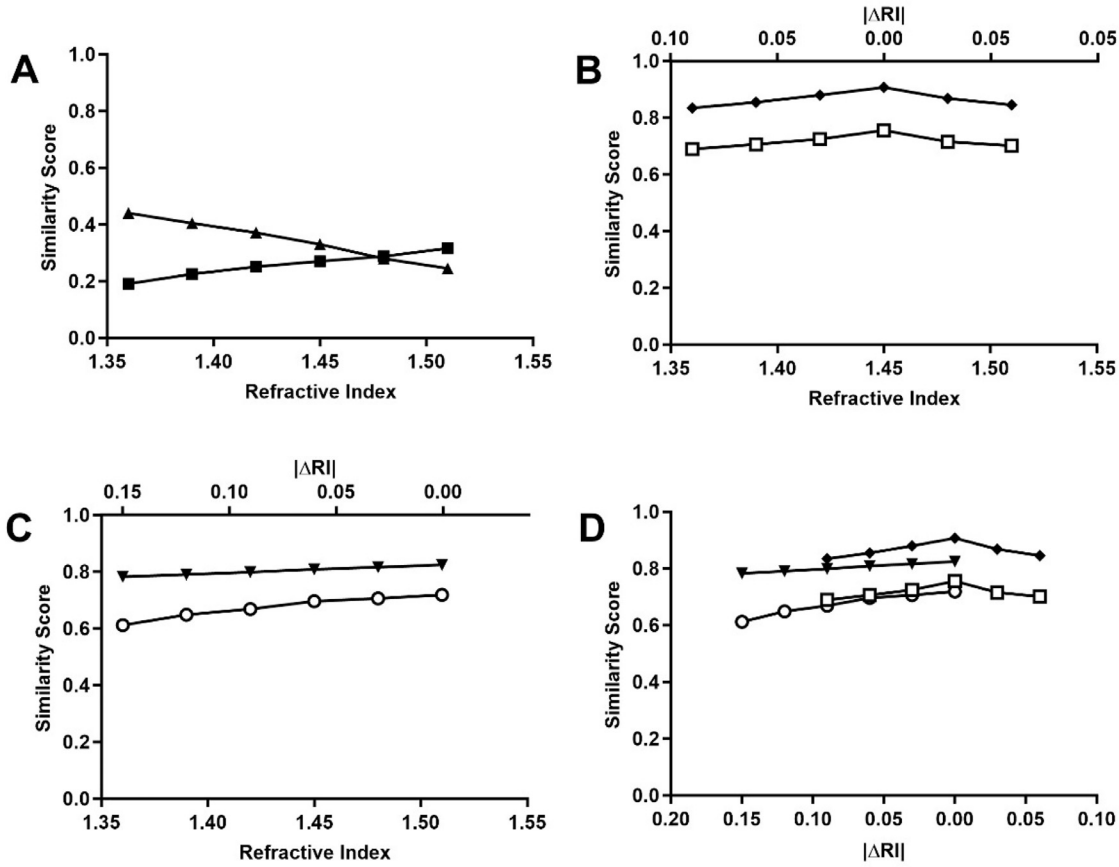

Figure 9. Effect of variation of the medium refractive index on image similarity score. A) PS spheres (filled squares, RI = 1.59), SU-8 (upward triangles, RI = 1.60). B) Particles produced by 2PP printing from IP-PDMS (RI = 1.45, filled diamonds: Model A, open squares: Model B). C) Particles produced by 2PP printing from IP-S (RI = 1.51, downward triangles: Model A, open circles: Model B). D) Image similarity of 2PP printed particles depending on differential refractive index (filled diamonds: IP-PDMS Model A, downward triangles: IP-S Model A, open squares: IP-PDMS Model B, open circles: IP-S Model B).

of SU-8 particles may be due to their outer and inner hole contours being more defined at lower ΔRI.

These results demonstrate that by using different materials and morphological designs, PLMPs can achieve high similarity to a heterogeneous protein particle dataset. This emphasizes the potential of PLMPs as a reference material that covers the variability of protein particles.

Sizing Accuracy of PLMPs

Particle length of protein-like standard particles obtained under conditions with a |ΔRI| > 0.03 by flow imaging microscopy are shown in Fig. 10. When ΔRI = 0, a significant decrease in particle length was observed due to matched refractive index between the particle and the matrix fluid (Fig. 7).[26] This effect is evident in Fig. 7C showing substantially smaller particles for IP-S, Model A at ΔRI = 0.

The average lengths of PLMPs are consistent with the scaling applied during the manufacturing process (Model A IP-S: 148 ± 22 μm; Model A IP-PDMS: 149 ± 16 μm; Model B IP-S: 156 ± 15 μm; Model B IP-PDMS: 157 ± 13 μm). The same is true for the particles printed in the subvisible range (not presented in this paper). It was assumed that there would be a higher variability of particle length for Model A, which has an elongated structure. However, analysis of the images acquired by flow imaging microscopy revealed that these particles preferentially oriented along the direction of flow in the flow cell. This may explain why length variability was similar to that of the more compact Model B. Nevertheless, some outliers that may correspond to particles of Model A in alternative orientation were observed as well.

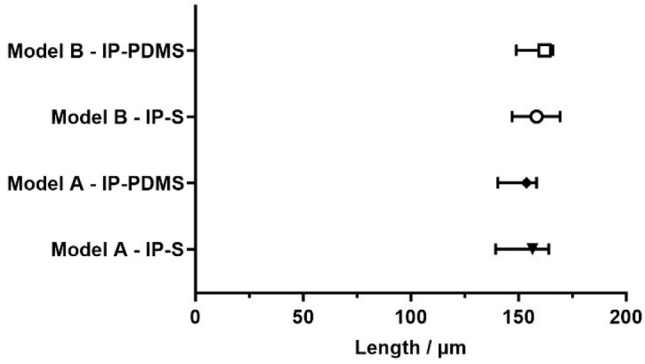

Figure 10. Median and interquartile range of length of protein-like particles printed with 2PP at |ΔRI| > 0.03.

Discussion

Within this study the morphological appearance as well as physical and optical properties of PS spheres, ETFE particles, SU-8 particles and novel PLMP were compared to proteinaceous particles present in biopharmaceutical drug products.

PS spheres are spherical, solid, non-porous particles (Fig. 3). The substantial difference between the refractive indices of PS and aqueous formulations results is high optical contrast (Fig. 4). Furthermore, the density of polystyrene (1.05 g/mL) results in a low sedimentation velocity in aqueous formulations. These attributes facilitate the

preparation of PS sphere suspensions that are easily detectable by analytical instruments with unequivocal sizing and reliable determination of particle concentration.[27] However, the morphological and optical characteristics of protein particles in biopharmaceutical formulations are unlike those of PS spheres, resulting in issues with regards to sizing and counting of proteinaceous particles.

Despite their morphological resemblance to protein particles (Fig. 6), a significant disadvantage of ETFE particles is their high density (1.70 g/mL), resulting in fast sedimentation in aqueous formulations which may pose problems with regards to sample handling and data interpretation.[11,23] Furthermore, due to the preparation process it is difficult to prepare particle suspensions at a defined concentration or size, which limits the application as particle standard.

SU-8 particles are unique with regards to their appearance and optical contrast (Fig. 6). On the one hand, the preparation process results in thin, sheet-like particles of well-defined size and morphology, which have been described as “floating mirrors” due to their morphology and high reflectivity.[27] On the other hand, SU-8 material is characterized by a high refractive index, which would typically result in dark particles when imaged in aqueous formulations (comparable to PS spheres). However, the low thickness of these particles in combination with their porous structure results in particles showing an optical contrast which is very similar to protein particles and virtually independent of variation of refractive index difference between SU-8 material and the suspension medium (Fig. 8A). Nevertheless, their morphology and appearance does not closely resemble visible protein particles mainly due to their flat shape, homogenous appearance, and sharp edge contrast (Fig. 9A).

Particles manufactured by 2PP printing represent a promising alternative to the available particle standards by meeting the desirable properties of protein-like standard particles. The manufacturing method allowed to prepare particles in the size range of visible or subvisible particles based on user-defined 3D models at high resolution. This strategy not only allows precise control over the shape of each individual particle but also allows facile preparation of well-defined sets of different particle shapes as exemplified by Model A and Model B, representing the heterogeneity of morphology and optical contrast of protein particles.[8] Furthermore, this preparation technique affords precise control over the particle concentration since a specific number of particles can be printed per substrate.

Proteinaceous particles are characterized not only by their irregular shape but also by their specific optical appearance, which is due to the low refractive index difference between the particles and the surrounding biopharmaceutical formulation. Ideally, protein-like particles should match the refractive index of protein particles of 1.41.[8,25] This challenge can be met by proper selection of photoresins having a low refractive index and/or through adjustment of the refractive index of the suspension medium, such that a low refractive index difference is achieved. The effect of variation of the photoresins refractive index is apparent from Fig. 6. However, since refractive indices of both IP-S and IP-PDMS were higher than 1.41, the effect of variation of the refractive index of the suspension medium was investigated in detail. Data presented in Fig. 8B and 8C shows that the average intensity of PLMPs can be finely tuned through variation of the refractive index of the medium to and even beyond the average intensity of protein particles. The ability to independently modify both the 3D shape and the optical characteristics of PLMPs allows to closely mimic a wide range of different proteinaceous particles having different geometrical and optical characteristics (Fig. 9 B-D).

Lastly, the sedimentation velocity of proteinaceous particles is an important parameter, especially with regards to handling of particle suspensions and visual inspection. Proteinaceous particles are considered to be neutrally buoyant, *i.e.* having a density close to that of the protein formulation.[28] The mass density of proteins has been theoretically and experimentally determined to be 1.22 g/mL to 1.43 g/mL.[29,30] However, the overall density of proteinaceous particles is substantially lower due to their high water content and was estimated to be 1.07 g/mL $\pm$ 0.05 g/mL using resonant mass measurement in combination with flow imaging microscopy.[30] The density of biopharmaceutical formulations varies depending on protein and excipient concentration. As an example, the density of mAb formulation 1 was determined to be 1.047 g/mL at 20°C. The densities of IP-PDMS (1.05 g/mL) and IP-S (1.11 g/mL) are within the range of protein particle density. The ability to define the 3D structure of PLMPs in conjunction with protein particle-like density of photoresins may allow to precisely mimic the sedimentation behaviour of protein particles.

The PLMPs established herein may find application as standard particles both for visible and subvisible particle characterization in biopharmaceutical formulations and beyond. With regards to characterization of subvisible particles, PLMPs may be employed as standard particles for light obscuration or flow imaging microscopy in addition to PS spheres. Sets of homogeneous PLMPs with known characteristics such as concentration, size, shape, and transparency may allow to improve instrument calibration resulting in accurate counting and sizing protein particles. Meanwhile, carefully selected mixtures of PLMPs with different sizes and shapes may be employed to monitor instrument performance over time. Moreover, PLMPs could serve as valuable tools for exploring new analytical instruments, developing novel analytical methods, and evaluating comparability of performance across different instruments. As an example, performance evaluation of backgrounded membrane-imaging (an alternative technique for analysis of subvisible particles) proved to be challenging because of rolling and pooling of PS spheres during filtration.[31–33] Another consideration is the possibility of future instruments capable of 3D particle characterization, which will create the need for a particle standard of known irregular 3D shape.

With regards to the visible range, the need for universal visible training kits, including visible protein-like particles, to reduce subjectivity associated with visual appearance testing has been emphasized.[34] Both, ETFE and SU-8 visible particles received mixed ratings due to their high sedimentation velocity (ETFE) or their high reflectivity and sharp edges (SU-8) in a recent interlaboratory study.[13] PLMPs have been shown herein to have improved properties rendering PLMPs potentially better suited for implementation in visual appearance training kits and for qualification of visual inspection methodologies. The accurate control over particle shape and size afforded by 2PP printing potentially allows to prepare specific training sets to train inspectors to detect and identify protein particles in closed container and may offer the opportunity to improve the definition of the lower detection limit of visible protein particle size. Semi-quantitative scales, composed with PLMPs having different size and concentration, may also be used to assess the level of visible protein particles in biopharmaceutical formulation.

Conclusion

Two-photon polymerization printing is a promising strategy for the fabrication of reference material mimicking the morphological, optical, and physical properties of protein particles. The refractive indices and densities of the photoresins employed in this study are similar to those of protein particles, resulting in similar optical and sedimentation properties. The flexibility offered by 3D printing allows obtaining particle morphologies and optical contrast very similar to protein particles and mimicking the natural variability of these properties. In addition, PLMPs size and concentration can be precisely controlled, which is a prerequisite for the certification of particle standards. The application of PLMPs may facilitate a better understanding and a proper evaluation of the performance of well-established and new instruments and methods for subvisible protein

particle characterization. A visible PLMP standard may enable better training and detection of product- or formulation specific protein particles and help alignment of current practices of visual inspection of protein particles in biopharmaceutical formulations. We believe that the use of PLMPs will facilitate harmonization and standardization of protein particle characterization across laboratories and organizations.

Declaration of Competing Interest

The authors declare that they have no known competing financial interests or personal relationships that could have appeared to influence the work reported in this paper.

Acknowledgement

The authors would like to thank the members of the Joint Particle Lab, F. Hoffmann-La Roche, Basel for analytical support and input. Furthermore, we thank Carmen Lema Martinez (F. Hoffmann-La Roche) for supporting this study, Georgios Imanidis (FHNW) for valuable discussions and support, and Dean Ripple (NIST) for providing the ETFE and SU-8 particles.

Supplementary Materials

Supplementary material associated with this article can be found, in the online version, at doi:10.1016/j.xphs.2024.04.011.

References

1. Barnard JG, Babcock K, Carpenter JF. Characterization and quantitation of aggregates and particles in interferon-β products: potential links between product quality attributes and immunogenicity. *J Pharm Sci*. 2013;102(3):915–928. https://doi.org/10.1002/jps.23415.
2. Melchore JA. Sound practices for consistent human visual inspection. *AAPS PharmSciTech*. 2011;12(1):215–221. https://doi.org/10.1208/s12249-010-9577-7.
3. Mazaheri M, et al. Monitoring of visible particles in parenteral products by manual visual inspection—reassessing size threshold and other particle characteristics that define particle visibility. *J Pharm Sci*. 2024;113(3):616–624. https://doi.org/10.1016/j.xphs.2023.10.002.
4. "<1787>Measurement of Subvisible Particulate Matter in Therapeutic Protein Injections," in United States Pharmacopoeia. Accessed: Feb. 13, 2023. [Online]. Available: https://doi.usp.org/USPNF/USPNF_M7866_03_01.html.
5. "<1>Injections," in United States Pharmacopoeia.
6. "<1788>Methods for the Determination of Particulate Matter in Injections and Ophthalmic Solutions," in United States Pharmacopoeia.
7. Ripple DC, Dimitrova MN. Protein particles: what we know and what we do not know. *J Pharm Sci*. 2012;101(10):3568–3579. https://doi.org/10.1002/jps.23242. Oct..
8. Matter A, et al. Variance between different light obscuration and flow imaging microscopy instruments and the impact of instrument calibration. *J Pharm Sci*. 2019;108(7):2397–2405. https://doi.org/10.1016/j.xphs.2019.02.019.
9. Kiyoshi M, et al. Collaborative study for analysis of subvisible particles using flow imaging and light obscuration: experiences in japanese biopharmaceutical consortium. *J Pharm Sci*. 2019;108(2):832–841. https://doi.org/10.1016/j.xphs.2018.08.006.
10. Ripple DC, Hu Z. Correcting the relative bias of light obscuration and flow imaging particle counters. *Pharm Res*. 2016;33(3):653–672. https://doi.org/10.1007/s11095-015-1817-9.
11. Ripple DC, Montgomery CB, Hu Z. An interlaboratory comparison of sizing and counting of subvisible particles mimicking protein aggregates. *J Pharm Sci*. 2015;104(2):666–677. https://doi.org/10.1002/jps.24287.
12. Sharma DK, King D, Merchant C. Reference material development for calibration and verification of image-based particle analyzers. *Int J Pharm*. 2011;416(1):293–295. https://doi.org/10.1016/j.ijpharm.2011.05.078.
13. Telikepalli SN, et al. An interlaboratory study to identify potential visible protein-like particle standards. *AAPS PharmSciTech*. 2022;24(1):18. https://doi.org/10.1208/s12249-022-02457-9.
14. Cash PW, Narwal R, Levitskaya SV, Krause S, Murphy D, Mazaheri M. Semi-quantitative analysis of inherent visible particles for biopharmaceutical products. *PDA J Pharm Sci Technol*. 2016;70(2):134–142. https://doi.org/10.5731/pdajpst.2015.006064.
15. Singh SK. Particulate matter in sterile parenteral products. In: Kolhe, Shah, Rathore, eds. *Sterile Product Development: Formulation, Process, Quality and Regulatory Considerations*. New York, NY: Springer; 2013:359–409. https://doi.org/10.1007/978-1-4614-7978-9_14. AAPS Advances in the Pharmaceutical Sciences Series.
16. Telikepalli S, Gonzalez K, Dragulin-Otto S, Ripple D, Carrier M, Khan M. Development of protein-like reference material for semiquantitatively monitoring visible proteinaceous particles in biopharmaceuticals. *PDA J Pharm Sci Technol*. 2019;73(5):418–432. https://doi.org/10.5731/pdajpst.2018.008953.
17. Ishii-Watabe A, et al. Recent achievements and current interests in research on the characterization and quality control of biopharmaceuticals in Japan. *J Pharm Sci*. 2020;109(5):1652–1661. https://doi.org/10.1016/j.xphs.2020.01.001.
18. Ripple D, et al. *Reference Material 8634:: Ethylene Tetrafluoroethylene for Particle Size Distribution and Morphology*. Gaithersburg, MD: National Institute of Standards and Technology; 2019. https://doi.org/10.6028/NIST.SP.260-193. NIST SP 260-193.
19. Cavicchi RE, et al. Particle shape effects on subvisible particle sizing measurements. *J Pharm Sci*. 2015;104(3):971–987. https://doi.org/10.1002/jps.24263.
20. Bunea A-I, del Castillo Iniesta N, Droumpali A, Wetzel AE, Engay E, Taboryski R. Micro 3D printing by two-photon polymerization: configurations and parameters for the nanoscribe system. *Micro*. 2021;1(2): 2. https://doi.org/10.3390/micro1020013. Art. no.
21. E. Freund and S. Cao, "Visible and subvisible protein particle inspection within a QbD-based strategy," in *Quality by Design for Biopharmaceutical Drug Product Development*, F. Jameel, S. Hershenson, M. A. Khan, and S. Martin-Moe, Eds., in AAPS Advances in the Pharmaceutical Sciences Series., New York, NY: Springer, 2015, pp. 331–352. https://doi.org/10.1007/978-1-4939-2316-8_15.
22. McGrory MR, King MD, Ward AD. Using mie scattering to determine the wavelength-dependent refractive index of polystyrene beads with changing temperature. *J Phys Chem A*. 2020;124(46):9617–9625. https://doi.org/10.1021/acs.jpca.0c06121.
23. Shibata H, et al. A collaborative study on the classification of silicone oil droplets and protein particles using flow imaging method. *J Pharm Sci*. 2022;111(10):2745–2757. https://doi.org/10.1016/j.xphs.2022.07.006.
24. Gross-Rother J, Blech M, Preis E, Bakowsky U, Garidel P. Particle detection and characterization for biopharmaceutical applications: current principles of established and alternative techniques. *Pharmaceutics*. 2020;12(11): 11. https://doi.org/10.3390/pharmaceutics12111112. Art. no.
25. Zölls S, et al. How subvisible particles become invisible—relevance of the refractive index for protein particle analysis. *J Pharm Sci*. 2013;102(5):1434–1446. https://doi.org/10.1002/jps.23479.
26. Hu Z, Ripple DC. The use of index-matched beads in optical particle counters. *J Res Natl Inst Stand Technol*. 2014;119:674–682. https://doi.org/10.6028/jres.119.029.
27. Telikepalli S, Ripple DC, Benkstein KD, Steffens KL, Carrier MJ, Montgomery CB. *Establishing Standards and Methods for Qualification and Validation of New Particle Measurement Technologies*. NIST; 2019... Accessed: Apr. 07, 2023. [Online]. Available: https://www.nist.gov/publications/establishing-standards-and-methods-qualification-and-validation-new-particle.
28. Freund E, Cao S. Visible and subvisible protein particle inspection within a QbD-based strategy. In: Jameel, Hershenson, Khan, Martin-Moe, eds. *Quality by Design for Biopharmaceutical Drug Product Development*. New York, NY: Springer; 2015:331–352. https://doi.org/10.1007/978-1-4939-2316-8_15. AAPS Advances in the Pharmaceutical Sciences Series..
29. Fischer H, Polikarpov I, Craievich AF. Average protein density is a molecular-weight-dependent function. *Protein Sci*. 2004;13(10):2825–2828. https://doi.org/10.1110/ps.04688204.
30. S. E. Zölls, "Protein particle analysis - critical factors and new standards".
31. Helbig C, Ammann G, Menzen T, Friess W, Wuchner K, Hawe A. Backgrounded Membrane Imaging (BMI) for high-throughput characterization of subvisible particles during biopharmaceutical drug product development. *J Pharm Sci*. 2020;109(1):264–276. https://doi.org/10.1016/j.xphs.2019.03.024.
32. Vargas SK, Eskafi A, Carter E, Ciaccio N. A comparison of background membrane imaging versus flow technologies for subvisible particle analysis of biologics. *Int J Pharm*. 2020;578: 119072. https://doi.org/10.1016/j.ijpharm.2020.119072.
33. Murphy MI, et al. Qualitative high-throughput analysis of subvisible particles in biological formulations using backgrounded membrane imaging. *J Pharm Sci*. 2022;111(6):1605–1613. https://doi.org/10.1016/j.xphs.2022.03.010.
34. Narhi L, Bou-Assaf GM, Gonzalez K, Mazaheri M, Messick S, Telikepalli S. *Filling the Pharmacopeial Gaps of Visual Inspection Toward Standardization and Consistency of Visible Particle Testing*. NIST; 2021... Accessed: Apr. 07, 2023. [Online]. Available: https://www.nist.gov/publications/filling-pharmacopeial-gaps-visual-inspection-toward-standardization-and-consistency.